Implementation and experimental validation of ultra-high speed PMSM sensor-less control by means of extended Kalman filter

Philipp Niedermayr, Luigi Alberti, *Senior Member, IEEE*, Silverio Bolognani, *Fellow, IEEE* and Reiner Abl

***Abstract*—This paper presents an experimental validation of the implementation of a sensor-less control algorithm for a ultra-high permanent magnet synchronous motor by means of an extended Kalman filter, up to 240 000rpm. The considered application is the air compressor for a fuel-cell in an electric car. It is shown that the extended Kalman filter can be used for the ultra-high speed drives, without any loss in accuracy and robustness. Proper experimental results are shown regarding the rotor position accuracy and dynamics of accelerations. The extendibility of the presented algorithm to different machines is shown by its implementation with nine different motors. In the paper also additional aspects such as the sensitivity of the algorithm towards changes in the back-EMF constant and the impact of temperature variations are considered.**

I. Introduction

In the recent years many applications call for the use of ultra-high speed (above 100krpm) permanent magnet synchronous motors (PMSM). Among them, their usage for air compressors in fuel cell vehicles is of special interest, as the advantages that come with high speed machines, such as an increased power per mass and volume ratio, are welcomed in any automotive application. Another advantage is the removal of the intermediate gearbox, with an increase of the system reliability and reduction of the maintenance costs. Due to mechanical constraints for the position sensors, high speed applications call for the development of efficient sensor-less control schemes.

However, while many studies propose sensor-less control speed schemes for low and medium speed PMSM, [1]–[4] among others, only few publications report drives in ultra-high speed regions. The application is challenging for the control scheme in terms of control accuracy [5] and computational time of the implementation [6], [7]. In the ultra-high speed operation also effects such as the iron losses [8], [9] and the non-linearities of the inverter due to dead times in the switching patterns [5] outweigh more than in the low-speed region and have to be considered and compensated.

Philipp Niedermayr is with Alpitronic GmbH, Bozen-Bolzano, Italy. Luigi Alberti and Silverio Bolognani are with the Department of Industrial Engineering, University of Padova, Padova, Italy (e-mail: edlab@dii.unipd.it). Reiner Abl is with BMW Group, Munich, Germany.

Due to this facts, other sensor-less control techniques for the ultra-high speed region have been generally used, such as open loop constant V/f or I/f techniques [11], DTC [5], adaptive control [10], [12]. More recently, also the Kalman filter has been considered in this application [13]–[15].

In this paper, we show that the usage of the EKF for ultra-high speed PMSM drives is feasible with good performance. In particular, the accuracy, dynamics and extendibility to a large number of different ultra high speed drives is shown by means of a detailed experimental validation on nine different prototypes. This makes the usage of EKF for the ultra-high speed drives interesting for a broad band of applications, especially in the automotive field.

Differently from low and medium speed applications, the control of ultra-high speed drives requires a very accurate and well-considered implementation of the algorithm on the hardware. Any inaccuracy in the implementation (execution order, measurement trigger, etc.) results in a rather large position error and hence instability and loss of efficiency. Therefore, the paper includes also the implementation details required by the specific application.

The paper starts with a short overview of the basics of the EKF as sensor-less control algorithm for a PMSM. The most important equations are reported and the experimental implementation and validation of the algorithm is reported in Sec. III. After a short description of the experimental setup, the EKF implementation is analysed regarding its accuracy (in terms of rotor position and speed), its parameters sensitivity, its dynamics (in terms of robustness of accelerations) and its maximum speed accomplished in this experiments. Section V, reports the considerations regarding the implementation of the algorithm.

II. The sensor-less control algorithm State of the art

The Kalman filter as a stochastic alternative to the Luenberger observer is a state of the art sensor-less control algorithm since many decades [17], [18]. Since the beginning of the the 90' the extended Kalman filter is used for the sensor-less control of electric machines [1]. As the emphasis of this publication is the experimental validation of the application of the Kalman filter for ultra-high speeds, the algorithm's equations are only briefly reported here. For the sake of completeness, the description of the

permanent magnet synchronous motor in the stator fixed stationary orthogonal reference frame is adopted, with the state variables:

$$\mathbf{x} = \begin{pmatrix} i_\alpha & i_\beta & \omega & \theta \end{pmatrix}^\intercal \tag{1}$$

with i_α and i_β corresponding to the stator currents in the α- and β-axis, ω the electrical angular frequency of the rotor and θ the electrical rotor position. Considering the process noise $\boldsymbol{\sigma}$ and the observation noise $\boldsymbol{\rho}$, the system equations can be written as:

$$\frac{\mathrm{d}}{\mathrm{d}t}\mathbf{x}(t) = \mathbf{A}\cdot\mathbf{x}(t) + \mathbf{B}\cdot\mathbf{u}(t) + \boldsymbol{\sigma} \tag{2}$$

$$\mathbf{y}(t) = \mathbf{C}\cdot\mathbf{x}(t) + \boldsymbol{\rho} \tag{3}$$

Here $\boldsymbol{\sigma}$ and $\boldsymbol{\rho}$ represent zero mean Gaussian noises with covariance matrices $\mathbf{Q}$ and $\mathbf{R}$ respectively. The input vector is $\mathbf{u} = (u_\alpha \quad u_\beta)^\intercal$, i.e. it is composed by the two phase voltages in the $\alpha-\beta$ reference frame. The output vector $\mathbf{y} = (i_\alpha \quad i_\beta)^\intercal$ is composed by the first two entries of state vector $\mathbf{x}$, yielding a simple matrix $\mathbf{C}$. The system describing matrix $\mathbf{A}$ and the input matrix $\mathbf{B}$ are given by:

$$\mathbf{A} = \begin{pmatrix} -\frac{R_s}{L_s} & 0 & \frac{\lambda_{mg}}{L_s}\sin\theta & 0 \\ 0 & -\frac{R_s}{L_s} & -\frac{\lambda_{mg}}{L_s}\cos\theta & 0 \\ 0 & 0 & 0 & 0 \\ 0 & 0 & \omega & 0 \end{pmatrix}, \quad \mathbf{B} = \begin{pmatrix} \frac{1}{L_s} & 0 \\ 0 & \frac{1}{L_s} \\ 0 & 0 \\ 0 & 0 \end{pmatrix} \tag{4}$$

with L_s the stator phase inductance ($L_s = L_d = L_q$ as only non-salient PMSM are considered), R_s the stator phase resistance and λ_{mg} the permanent magnet stator flux linkage.

By writing the system equation as difference equation, the predict step of the Kalman filter can be derived to

$$\hat{\mathbf{x}}_k^- = \underbrace{(\mathbf{1} + \mathbf{A}\cdot T_s)\cdot\hat{\mathbf{x}}_{k-1} + \mathbf{B}\cdot T_s\cdot\mathbf{u}_{k-1}}_{f(\hat{\mathbf{x}}_{k-1},\mathbf{u}_{k-1},0)} \tag{5}$$

and the correct step can be written as

$$\hat{\mathbf{x}}_k = \hat{\mathbf{x}}_k^- + \mathbf{K}_k(\mathbf{y}_k - \underbrace{\mathbf{H}\cdot\hat{\mathbf{x}}_k^-}_{\hat{\mathbf{y}}_k}) \tag{6}$$

where the matrices $\mathbf{K}_k$ is the Kalman gain and $\mathbf{H}$ denotes the Jacobian matrix [15].

The overall control algorithm is shown in Fig. 1. The PMSM is speed controlled with an outer speed control loop and the two inner d- and q- axis current control loops. According to maximum torque per Ampere operating conditions of non-salient PMSMs the d-axis current contol loop has a fixed target of zero, while the otput of the speed control loop is the target for the q-axis current control loop.

For the current control loops, the filtered α- and β axis currents are transformed into the d- and q-axis via the Park transformation using the estimated angle (experimental validation showed that taking the filtered currents is more robust against noise than taking the directly measured currents). The estimated speed is needed for the decoupling of the d- and q-axis as well as for the speed loop. Fig. 1 shows the described implementation details.

The start-up procedure for the application consists in an open-loop I/f mode ramp with a subsequent switching to the closed loop Kalman driven control.

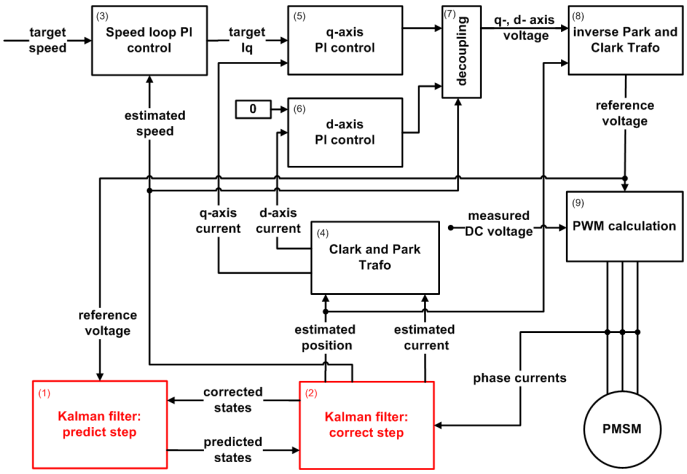

Fig. 1. The adopted field oriented control algorithm. The Kalman filter feeds the speed PI controller and the currents transformation. The numbers in the blocks indicate the execution order of the algorithm.

A. Parameterization of the control algorithm

One of the most challenging tasks in the implementation of the Kalman filter is the parametrization of the covariance matrices of the measurement noise $\mathbf{R}$ and the process noise $\mathbf{Q}$. Two different approaches for the parameterization were used for the different machines (see III-B).

For most of the machines, $\mathbf{Q}$ and $\mathbf{R}$ were parameterized via a trial and error method to $R_{11} = R_{22} = 4$, $Q_{11} = Q_{22} = 1$ and $Q_{44} = 1e-5$ (for all machines), while $Q_{33} = 0.05...0.1$ (adaption for every machine). As reported in [13] the algorithm's convergence is most sensitive to Q_{33}, which needed to be adjusted for every machine, while all other parameters could be kept constant. The parameters proofed to work fine in all operating conditions of the machines, hence also for the wide speed range from 30krpm to 150krpm.

A second method for the parameterization was adopted from [20], which consists in a normalization of the motor parameters and the EKF algorithm, with the obvious advantage of the re-usage of the parameters for the $\mathbf{R}$ and $\mathbf{Q}$ matrices in the normalized space. It was used for two different machines in the lower power range (up to 2kW).

III. Experimental setup and implementation

A. Description of the inverter

The inverter used for the validation of the implementation of the Kalman filter is a SiC-Mosfet inverter designed for a nominal phase current of 200Arms, and a maximum

DC voltage of 730V. The switching frequency was chosen to 40kHz, in order to be able to drive a maximum electrical frequency of 4kHz (corresponding to 240krpm for a 2-pole motor). In [5] the performance improvements of a SiC-inverter with respect to an inverter with conventional Si-IGBTs are listed. Among them the faster switching speed and the shorter dead-time can be emphasized, resulting in performance improvements due to lower THDi of the phase currents and less influence of the inverter non-linearities, respectively. In the experiments presented here a death time of $250ns$ was adopted (1% of the switching period). As the sampling time of the control algorithm is consistent with the switching frequency, the calculation time must not exceed 25μs. However, other than described in [7] the implementation was realized on a conventional DSP (instead of FPGA). As the control algorithm was implemented in MATLAB/SIMULINK and verified in a closed loop simulation model, it was coded with the MATLAB Embedded Coder (a method which speeds up the implementation time essentially). The algorithm was implemented with single-precision floating-point format and run at a clock frequency of 200MHz. Among the efforts to reduce the calcualtion time, the calculation of the matrices of the Kalman algorithm were conducted manually in order to uses symmetries and zero-entries to reduce the number of operations. The sinus-calculation was optimized by using a Taylor-approximation and the Embedded Coder was tuned for the target hardware. This resulted in an overall computation time of the algorithm of 13μs More details on the implementation order are given in Sec. V.

B. Description of the synchronous motor

One of the main points of this publication is to emphasize the applicability of the described control algorithm to a large number of synchronous motors. In effect up to now the control algorithm was tested on nine different machines with an essential variance of the machine parameters. Fig. 2 shows the distribution of the three most important motor normalized parameters: the permanent magent flux linkage λ_{mg}, the stator inductance L as well as their maximum speed. In the following only the results related to the most significant machines are reported for the sake of brevity. Nevertheless, similar results in terms of good performance and controllability have been achieved with all the motors. Fig. 3 shows a picture of a commercial compressor equipped with the high-speed motor adopted in the test.

IV. Experimental validation

A. Accuracy of the Kalman algorithm

The application of the present PMSM control calls for high accuracy in terms of rotor position and speed estimation. The accuracy directly influences the performance in control dynamics and efficiency (see Sec. V). Both, angle accuracy and speed accuracy were investigated. The speed accuracy was already presented in [15] while the angle accuracy is presented hereafter.

In an experiment performed with a machine equipped with Hall sensors, the rotor position estimated by the Kalman filter and the measured rotor position were compared. The results are plotted in Fig. 4. The estimated angle matches the real angle very well and hence allows high dynamics and efficiencies. Similar accuracy in the angle estimation can be observed also during transient operations, such as during start-up.

It is also important to mention that the rotor speed is calculated by the derivative of the rotor position $\omega = \frac{d\theta}{dt}$, which gives a very precise estimation of the revolution speed, as any constant position error does not affect the estimated speed.

B. Parameter sensitivity

The parameter sensitivity of the Kalman filter has been largely investigated on a theoretical basis in [19]. For the experimental validation performed for this publication, special interest has been given to the parameter sensitivity regarding the permanent magnet flux linkage λ_{mg}, as this parameter is exposed to potential variability with operating temperature.

As mentioned in Sec. IV-A calculating the revolution speed of the rotor in terms of the time derivative of the rotor position θ, gives a very accurate result, otherwise no successful synchronous operation would be possible. Hence by calculating the difference between the real speed ω_{real} (given by the time derivative of the angle) and the estimated speed by the Kalman filter ω_{Kalman} ($\Delta\omega = \omega_{real} - \omega_{Kalman}$), an online estimation of the difference between the real permanent magnet flux linkage $\lambda_{mg,real}$ and the permanent magnet flux linkage $\lambda_{mg,Kalman}$, fed to the Kalman filter ($\Delta\lambda_{mg} = \lambda_{mg,real} - \lambda_{mg,Kalman}$), can be calculated.

It is worth notice that ω_{real} is not measure by sensors but it is calculated online as derivative of the estimated position. The "real" attribute is used to highlight that its value is more accurate respect to the Kalman filter estimation ω_{Kalman}. In [19], a theoretical derivation shows that any error in the parameter of $\lambda_{mg,Kalman}$ is directly reflected on the speed error.

A detailed description of rotor losses occurring during operation of a high speed PMSM is given in [8]. Eddy current losses in the rotor lead to a rise in the rotor temperature which is very difficult to measure and monitor during operation. With a temperature increase, both, remanent flux density and coercitivity of the magnets decrease [21]. A change in the remanent flux density B_r of a magnet can be linked to the change of its temperature

$$\Delta T = \frac{1}{RTC} \cdot \frac{\Delta B_r}{B_r} \tag{7}$$

with RTC the reversible temperature coefficient of the magnet's material.

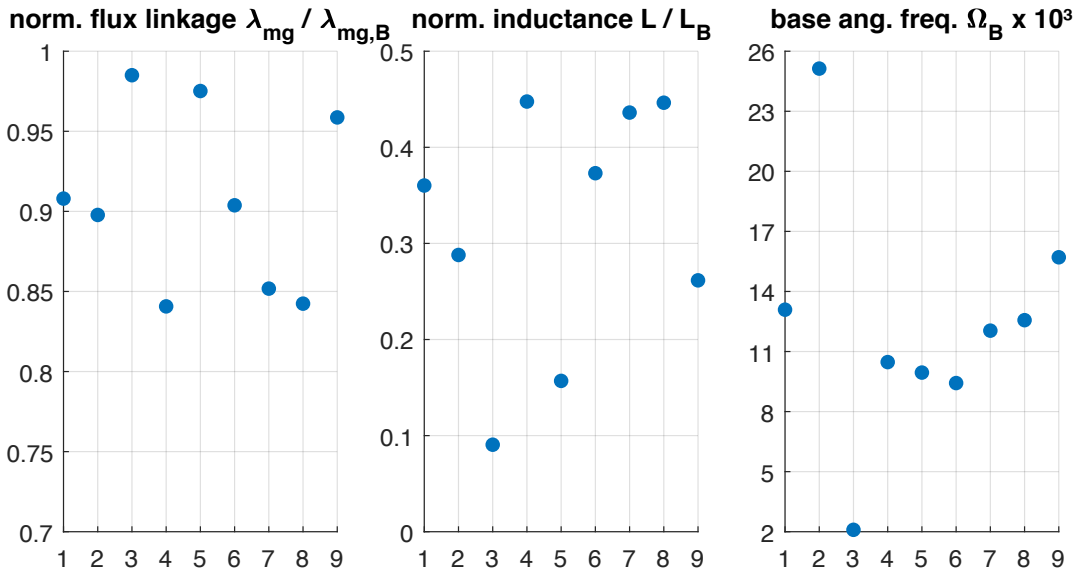

Fig. 2. The graphs show the distribution of the PMSM parameters of the nine different machines used for the validation of this publication. In order to be able to compare them, the parameters λ_{mg} and L_s were normalized by their base values $\lambda_{mg,B}$ and $L_{s,B}$ respectively [22]. For the maximum speed of the machines the absolute value is given.

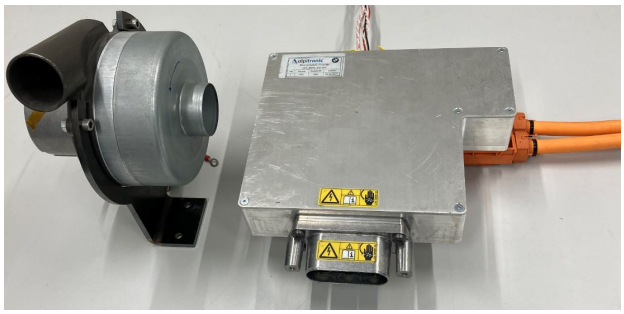

Fig. 3. A picture of a commercial motor coupled with a compressor adopted in the test. Nominal power is $1.1kW$

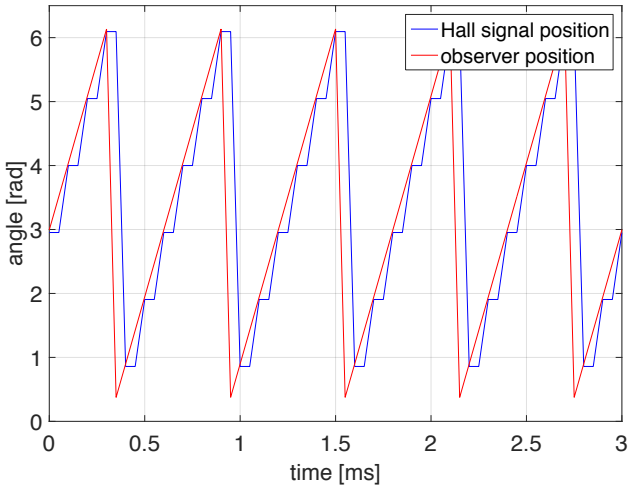

Fig. 4. Accuracy of the estimated rotor position. For the better comparison, the observer signal is plotted pseudo-continuous, although it is only updated at every calculation step (hence, with 40kHz in this case). The Hall signal is only updated for every $\theta = n \cdot \frac{\pi}{3}$ (with $n = 1, 2, ...$) as there are only three Hall sensors placed at every $\theta = \frac{2\pi}{3}$. The accuracy of the estimated angle can hence be compared to the real angle at the moment, the Hall signal gets updated.

Hence, by calculating the relative change of the Kalman estimated rotor speed to the real speed $\frac{\Delta\omega}{\omega}$, one obtains an online estimation of the rotor's temperature change ΔT

$$\Delta T \propto \frac{\Delta B_r}{B_r} \propto \frac{\Delta\lambda_{mg}}{\lambda} \propto \frac{\Delta\omega}{\omega} \tag{8}$$

Equation (8) reveals that this evaluation gives an estimation on the relative change of the permanent magnet flux linkage and hence the magnets temperature, rather than its absolute value. The absolute value is difficult to derive as there is never a perfect accordance between the real permanent magnet flux linkage and the value fed to the Kalman filter, i.e. $\Delta\lambda_{mg} \neq 0$ even at room temperature conditions at the very beginning of the motor operation. This is mainly caused by the inverter non-linearities.

During experimental validation of an PMSM equipped with temperature sensors in the stator, at a steady speed of 70krpm and 50krpm respectively, the change over time of the permanent magnet flux linkage $\frac{\Delta\lambda_{mg}}{\lambda}$ was estimated by the method described above and compared to the stator temperature measured in a spot close to the rotor. The results are reported in Fig. 5, with the measured stator temperature in blue and the online calculated $\frac{\Delta\omega}{\omega}$ in orange. The first plot shows a measurement at 70krpm: both curves show a first-order-low-pass behaviour. They

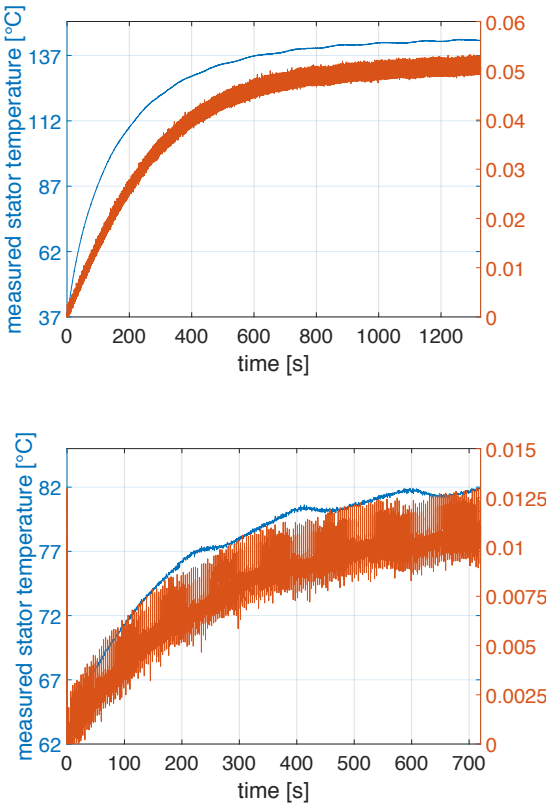

Fig. 5. A comparison between the measurement of the stator temperature on a spot close to the rotor in blue and the online calculated $\frac{\Delta\omega}{\omega}$ in orange at a steady speed of 70krpm (above) and 50krpm (below). Please note: The y-axis on the right hand side of the plots is given in a.u. as ratio $\frac{\Delta\omega}{\omega}$, the label is omitted. Both plots show a high similarity between the behavior of the stator temperature and the calculated $\frac{\Delta\omega}{\omega}$, even the oscillations present in the temperature signal in the lower plot can also be seen in the $\frac{\Delta\omega}{\omega}$-signal.

certainly have different time constants, because of the different origin of the temperature change (for the stator iron and copper losses dominate, while for the rotor eddy currents are the main source of temperature change). The second plot was measured at 50krpm: the oscillations in the measured temperature can also be seen in the calculated $\frac{\Delta\omega}{\omega}$. The oscillations can be caused on the test bench by a variation of the temperature of the compressor inlet air, which at this relatively low speed would have an effect on the rotor and the stator temperature.

It can hence be concluded, that the change of the value of the permanent magnet flux linkage can be estimated online and can be related to losses in the rotor and hence a temperature change of the magnet.

C. Dynamics of the control algorithm

Fig. 6 shows a dynamic step from 30krpm to 110krpm. The step response was performed in 730ms, with a maximum q-axis current of $280\mathrm{A}_{pk}$ during the acceleration. The medium acceleration slope corresponds to $116\frac{\mathrm{krpm}}{\mathrm{s}}$. Newest tests with a different machine even reached acceleration slopes of $200\frac{\mathrm{krpm}}{\mathrm{s}}$, however, still at cost of the stability.

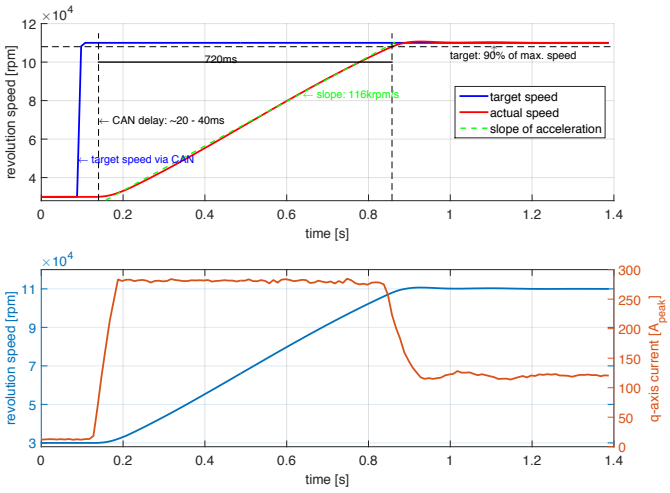

Fig. 6. Step response of the speed control for a step from 30krpm to 110krpm, performed in 730ms; above: target speed and estimated speed as a function of time; below: related q-axis current and estimated speed. The acceleration current of $280\mathrm{A}_{pk}$ corresponds to the inverter's limit.

In Fig. 7 a start-up procedure from zero speed to idle speed (30 000rpm in this case) is shown. As mentioned in Sec. II, for the start-up of the PMSM an open loop I/f control algorithm was used for the low speed region. Due to the unknown initial rotor position, the frequency is increased slowly for the first 150ms after the start. This makes sure, the rotor is aligned to the electrical angle imposed by the I/f mode. After this sort of home-positioning, the frequency is increased faster, before the start-up algorithm switches to the closed loop Kalman-driven control. This occurs at $t = 0.55$s (at a speed of approx. 15krpm), which is manifested by a peak in the estimated rotor speed. It is an artifact of the Kalman filter at the moment the control loop is closed with the Kalman's speed and position and does not correspond to the real speed at this moment. However the start-up procedure is stable and reproducible without any failed start-ups and is concluded within 630ms. The start-up time could even be improved. However this goes at the cost of reproducibility by increasing the probability of a failed start-up event. Fig. 7 also shows the q-axis current during the start-up. As can be clearly seen, the controlled current is very stable in the low speed region, but suffers an increasing oscillation at higher speeds. This kind of oscillation can also be observed with the V/f-method (where it behaves even worse). As the electrical angle during the open loop control is imposed, a possible cause of this could be an oscillation of the real rotor position around the imposed electrical angle. After the switching procedure to the Kalman driven algorithm the current is stable again.

D. Drive at 240 000rpm

To prove the Kalman filter's performance at ultra-high speeds, a prototype with a maximum revolution speed of 240 000rpm (at an electrical power of $\approx$ 1.5kW) was successfully driven on the test bench. In difference to the

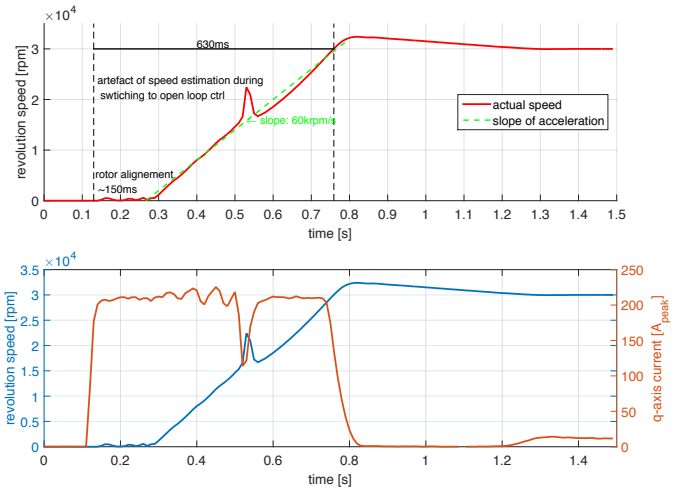

Fig. 7. Start-up from zero to idle speed. See text for details.

other prototypes presented in this paper, for this one the Kalman was normalized, as described detailed in [20] and Sec. II-A. Fig. 8 shows a screenshot of the oscilloscope measuring the phase currents at steady state maximum speed.

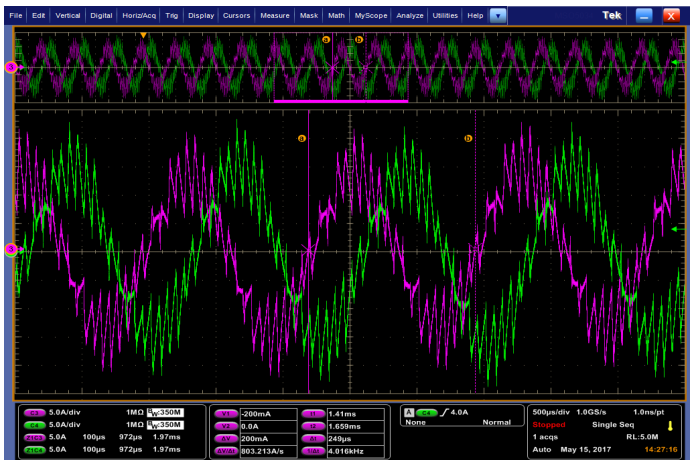

Fig. 8. Phase currents measured with an oscilloscope at the maximum speed of 240krpm. The electrical frequency of 4kHz, corresponds to one tenth of the PWM switching frequency, which is manifested in a distorted phase current.

V. Implementation of the Kalman Filter

Introducing the equations of the Kalman Filter reported in Sec. II, no considerations regarding the implementation on a real hardware were made. For low speed applications, where the ratio between the switching frequency and the fundamental electrical frequency is large, a wrong implementation of the Kalman Filter has a minor effect on its accuracy. However, as this paper deals with high speed applications, where the ratio between switching frequency and fundamental electrical frequency is small (down to a ratio of 10), even small errors in the calculation of the rotor angle result in essential distortions of current and voltages. Most modern inverter implementations make use of the center aligned PWM method and measure the phase currents at the center of the modulation period. This is shown schematically in Fig. 9(a): each of the three duty cycles is applied symmetrically around the center of the period, i.e. the ON-time in the first half of the switching period (here called PWM period) is the same as in the second half of the period. The phase currents are measured at the center of the PWM period, i.e. after half of the time, the voltages are applied to the stator.

The instants of measurement of the phase currents, representing the two states i_α and i_β (see (1)) define the calculation periods in which the difference equation (5) holds. The second addend in (5) represents the external input to the system during the calculation period. As can be immediately seen in Fig. 9(a), there is a mismatch between the calculation period for which the difference equation (5) holds and the PWM period representing the system inputs u_α and u_β. If this mismatch isn't corrected, it can introduce essential errors in the calculation of the rotor position θ [23].

Fig. 9(b) shows one possible solution to overcome the problem: here (5) has to be modified giving the following expression:

$$\hat{\mathbf{x}}_k^- = (\mathbf{1}+\mathbf{A}\cdot T_s)\cdot\hat{\mathbf{x}}_{k-1}+\frac{\mathbf{B}\cdot T_s\cdot\mathbf{u}_{k-2}}{2}+\frac{\mathbf{B}\cdot T_s\cdot\mathbf{u}_{k-1}}{2} \quad (9)$$

In order to match the applied voltages to the calculation period, the mean of the voltages of the PWM period $k-2$ and the PWM period $k-1$, has to be taken for the system input.

Another possibility to match the calculation period with the PWM period, is more obvious and consists in moving the moment of the current acquisition from the center of the period to the edge of the period (see Fig. 9(c)). Now the period during the PWMs are applied match the period for which the filter algorithm is calculated and the correction 9 must not be applied. The difference between the two methods of correction is the digital delay. While for the method shown in Fig. 9(b)) the delay is only half of a period, 9(c)) delays the output of the control algorithm for an entire period.

In both cases, however, there is another angle correction to be made, which again has essential influence on the performance of high speed applications: the Kalman filter's state vector as given in (1) doesn't represent the 4 states for the same time instant. Again (5) has to be considered: starting from the currents $i_{\alpha,k-1}$ and $i_{\beta,k-1}$ the currents $i_{\alpha,k}$ and $i_{\beta,k}$ are calculated out of the two voltage contributions (neglecting for the moment the resistive voltage drop), the external voltage and the back-EMF voltage. As one can see, they depend on the angle θ, the third entry of the state vector of (1). It is clear, that in order to match the back-EMF voltage to the calculation period, for θ the angle in the center of the calculation period has to be taken. This means, that the two currents are always calculated for the edge of the calculation period, while the rotor angle is calculated for the center of the calculation period.

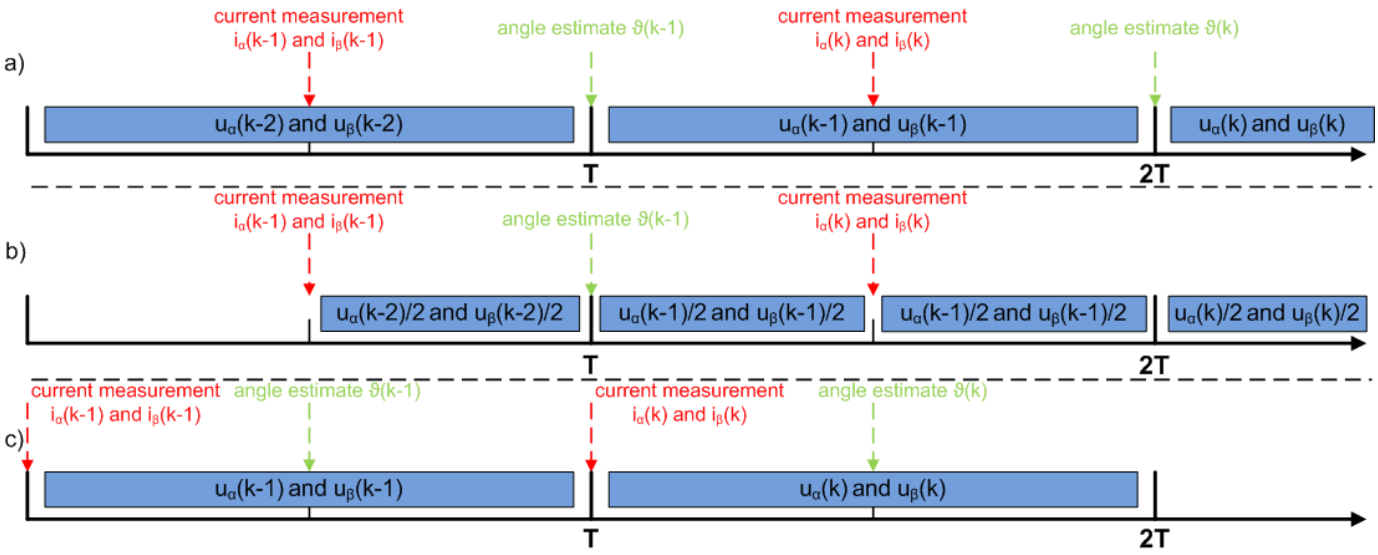

Fig. 9. (a) Center aligned PWM and centered current acquisition. The reference voltage for the Kalman predict step corresponds to the PWMs in the respective period.
(b) Correction according to Eq. 9: Center aligned PWM and centered current acquisition. The reference voltage for the Kalman corresponds to the mean of the PWMs of two consecutive periods, hence the applied voltages are matched to the calculation period.
(c) Center aligned PWM, but current acquisition at the edge of the PWM period. Here the applied voltages match the calculation period without a correction. However, this comes at the cost of a longer digital delay.

At the moment the angle θ is handed over from the Kalman Filter to the FOC current control, this has to be taken into account when calculating the Park transformations. This can be done by shifting the angle for the Park transformation of the phase currents by half a period to the left $\theta^* = \theta_k - \omega \cdot \frac{T}{2}$ and the angle for the inverse Park transformation for the target phase voltages by
- half a period to the right $\theta^* = \theta + \omega \cdot \frac{T}{2}$ for the centered current aquisition (Fig. 9(b)) and
- by an entire period to the right $(\theta^* = \theta + \omega \cdot T)$ for the current aquisition a the edge of the period (Fig. 9(c)).

The above considerations regarding the implementation of the Kalman Filter have proven to work fine both in simulation and on the test bench. Fig. 10 compares the q-axis current of the drive needed for different speeds, with and without the above described corrections.

In this case, the switching frequency was 40kHz and the electrical frequency up to 2kHz, i.e. in one calculation step, the rotor performs a rotation of $\frac{\pi}{10}$. Without the corrections, the estimated angle is off by $\frac{\pi}{10}$. This means, that if the torque demand requires a q-axis current of e.g. 100A, a d-axis current of $100\text{A} \cdot \sin(\frac{\pi}{10}) = 30\text{A}$ is imposed, which does not produce any torque.

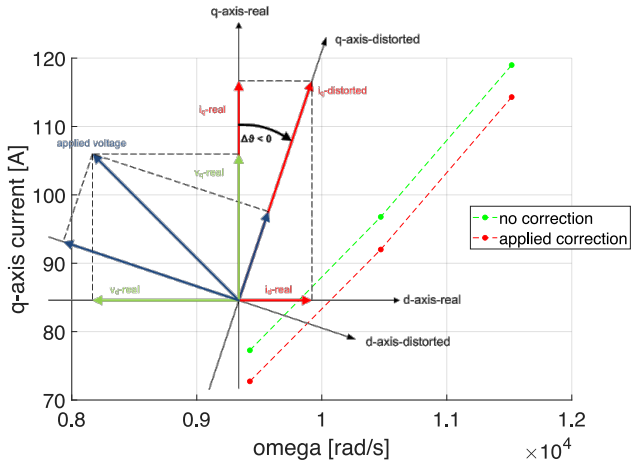

Fig. 10. Experimental results to show the benefit obtained by the proposed correction. The plot shows the q-axis-current needed to drive the compressor at different speeds. It compares the q-axis current needed, in the two cases: if the above described correction is applied and if there is no correction made. The load at the given speeds was the same in both cases. As can be seen in the inset, if there is an angle distortion $\Delta\theta = \theta - \hat{\theta}_k$ between the real rotor angle θ and the estimated rotor angle $\hat{\theta}_k$, the q-axis current in the distorted reference frame produces a d-axis-current in the real reference frame, which does not produce any torque, but only losses.

VI. Conclusion

In this paper the successful experimental implementation of the EKF for PMSM in the ultra-high speed region was shown. The implementation was tested on a large number of different machines, which proves its easy adaptability for different parameter sets. The control algorithm shows a good quality regarding the rotor position and speed accuracy and is well suited for applications which demand high dynamics. A maximum speed of 240 000rpm has been achieved. It was shown, that the presented algorithm can deliver also online information about the relative change of the rotor temperature, which is particularly important for ultra-high speed applications.

References

[1] A. Bado, S. Bolognani and M. Zigliotto, "Effective estimation of speed and rotor position of a PM synchronous motor drive by

a Kalman filtering technique", in Power Electronics Specialists Conference, 1992. PESC '92 Record., 23rd Annual IEEE, 1992, S. 951–957 Bd.2.
[2] S. Bolognani, R. Oboe and M. Zigliotto, "Sensorless full-digital PMSM drive with EKF estimation of speed and rotor position", IEEE Transactions on Industrial Electronics, Vol. 46, Is. 1, pp. 184–191, Feb. 1999.
[3] A. Qiu, B. Wu and H. Kojori, "Sensorless control of permanent magnet synchronous motor using extended Kalman filter", in Canadian Conference on Electrical and Computer Engineering, 2004, Vol. 3, pp. 1557-1562.
[4] Heui-Wook Kim and Seung-Ki Sul, "A new motor speed estimator using Kalman filter in low-speed range", IEEE Transactions on Industrial Electronics, 1996, pp. 498-504, Vol. 43 Is. 4,
[5] R. Togashi, Y. Inoue, S. Morimoto and M. Sanada, "Performance improvement of ultra-high-speed PMSM drive system based on DTC by using SiC inverter", in proceedings of International Power Electronics Conference (IPEC-Hiroshima-ECCE ASIA), 2014, pp. 356–362.
[6] L. Sepulchre, M. Fadel and M. Pietrzak-David, "Improvement of the digital control of a high speed PMSM for vehicle application", Eleventh International Conference on Ecological Vehicles and Renewable Energies (EVER), 2016, pp. 1–9.
[7] S. Konaka, Y. Inoue, S. Morimoto and M. Sanada, "Comparative study of control characteristics in ultra-high-speed PMSM drives", inproceedings of 5th IEEE International Symposium on Sensorless Control for Electrical Drives, 2014, pp. 1–6.
[8] J. Kim, I. Jeong, K. Nam, J. Yang and T. Hwang, "Sensorless Control of PMSM in a High-Speed Region Considering Iron Loss", IEEE Transactions on Industrial Electronics, 2015, Vol. 62, Is. 10, pp. 6151–6159.
[9] S. Yamamoto, H. Hirahara, A. Tanaka, T. Ara and K. Matsuse, "Universal Sensorless Vector Control of Induction and Permanent-Magnet Synchronous Motors Considering Equivalent Iron Loss Resistance", IEEE Transactions on Industry Applications, 2015, Vol. 51, Is. 2, pp. 1259–1267.
[10] D. Gerada, A. Mebarki, N. L. Brown, C. Gerada, A. Cavagnino and A. Boglietti, "High-Speed Electrical Machines: Technologies, Trends, and Developments", IEEE Transactions on Industrial Electronics, 2014 , Vol. 61, Is. 6, pp. 2946–2959.
[11] L. Xu and C. Wang, "Implementation and experimental investigation of sensorless control schemes for PMSM in super-high variable speed operation", in proceedings od Thirty-Third IEEE IAS Annual Meeting, 1998, Vol. 1, pp. 483–489.
[12] J. Lee, "Adaptive sensorless control of high speed PMSM with back EMF constant variation", in proceedings of 9th International Conference on Power Electronics and ECCE Asia (ICPE-ECCE Asia), 2015, pp. 1400–1404.
[13] S. Bujacz, A. Cichowski, P. Szczepankowski and J. Nieznanski, "Sensorless control of high speed permanent-magnet synchronous motor", in proceedings of 18th International Conference on Electrical Machines, 2008, pp. 1–5.
[14] A. Cichowski, S. Bujacz, J. Nieznanski and P. Szczepankowski, "Sensorless startup of super high speed permanent magnet motor", in proceedings of IEEE International Symposium on Industrial Electronics (ISIE), 2010 , pp. 3101–3106.
[15] P. Niedermayr, S. Bolognani, L. Alberti and R. Abl, "Sensorless control of a super-high speed synchronous motor drive based on a Kalman filter", in proceedings of 42nd Annual Conference of the IEEE Industrial Electronics Society, 2016, pp. 1870–1875.
[16] P. Niedermayr, L. Alberti, S. Bolognani and R. Abl, "High speed sensorless control of a synchronous motor with Kalman filter", in proceedings of International Exhibition and Conference for Power Electronics, Intelligent Motion, Renewable Energy and Energy Management, PCIM 2016, pp. 1–9.
[17] R. E. Kalman, "A New Approach to Linear Filtering and Prediction Problems", Journal of Basic Engineering, Vol. 82, Is. 1, pp. 35–45, March 1960.
[18] D. Simon, "Optimal state estimation", Wiley, 2006
[19] S. Bolognani and M. Zigliotto, "Parameter sensitivity of the Kalman filter applied to a sensorless synchronous motor drive", in proceedings of EPE'95 conference, 1995, Vol. 3, pp. 375–380.
[20] S. Bolognani, L. Tubiana and M. Zigliotto, "Extended Kalman filter tuning in sensorless PMSM drives", IEEE Transactions on Industry Applications, 2003, Vol. 39, Is. 6, pp. 1741–1747.
[21] S. Jumayev, M. Merdzan, K. O. Boynov, J. J. H. Paulides, J. Pyrhönen and E. A. Lomonova, "The Effect of PWM on Rotor Eddy-Current Losses in High-Speed Permanent Magnet Machines", IEEE Transactions on Magnetics, 2015, Vol. 51, Is. 11, pp. 1–4.
[22] N. Bianchi ; S. Bolognani, "Parameters and volt-ampere ratings of a synchronous motor drive for flux-weakening applications" IEEE Transactions on Power Electronics, 1997, Vol. 12, Iss. 5, pp. 895-903
[23] Myoungho Kim, Jung-Sik Yim, Seung-Ki Sul and Sung-Il Lim, "Implementation of super high-speed permanent magnet synchronous machine drive", IEEE Energy Conversion Congress and Exposition, 2009, pp. 1700 - 1704

Philipp Niedermayr graduated in physics at the Technical University of Munich in 2014 and joined Alpitronic company, Bolzano, Italy, in the same year. There he is with the system development department and mainly works on control algorithms and power loss simulations for high power converters and as a project manager for power electronic components in electrical vehicles and charging stations.

Luigi Alberti (S'07-M'09-SM'20) received the Laurea and the Ph.D. degrees in electrical engineering from the University of Padova, Padova, Italy, in 2005 and 2009, respectively. From 2009 to 2012, he was a Research Associate at the University of Padova. In 2012, he moved to the Faculty of Science and Technology, Free University of Bozen-Bolzano, Italy, to start research and educational activities in the field of electrical engineering and electrical machines. He is currently an Associate Professor with the Department of Industrial Engineering, University of Padova, working on design, analysis, and control of electric machines and drives, with particular interest in renewable energies and more electric vehicles.

Silverio Bolognani (F '19) received the Laurea degree in electrical engineering from the University of Padova, Padova, Italy, in 1976. He was the Head of the Department of Electrical Engineering, from 2001 to 2008, Member of the Scientific Committee from 2004 to 2008, Vice-Rector for the Department of Research from 2009 to 2015 with the University of Padova. He is currently a Full Professor of electrical converters, machines and drives with the same university. He is the Author of three patents and more than 250 international publications. Prof. Bolognani is a Chairman of the IEEE IAS/IES/PELS North Italy Joint Chapter and Member of the Scientific Committee of National and International Conferences and Associations.

Reiner Abl graduated as electrical engineer (Dipl.-Ing.) at the University of Applied Sciences Würzburg-Schweinfurt in 1999. His employment experience includes Siemens AG (Central technology), IQ-Mobil (Startup), Altran, Audi AG and currently BMW Group. He mainly worked in the field of digital signal processing in the field of high frequency application as well as in power electronic applications. His current position is project manager for power electronic in fuel cell vehicles in the department of advanced development for e-drive trains.